Hydrol. Earth Syst. Sci. Discuss., 10, 3629–3664, 2013
www.hydrol-earth-syst-sci-discuss.net/10/3629/2013/
doi:10.5194/hessd-10-3629-2013

Hydrology and Earth System Sciences
Open Access
Discussions

Large scale snow water status monitoring: comparison of different snow water products in the upper Colorado basins

G. A. Artan[1], **J. P. Verdin**[2], **and R. Lietzow**[2]

[1]ASRC Research and Technology Solutions, Contractor to the US Geological Survey (USGS) Earth Resources Observation and Science (EROS) Center, Sioux Falls, SD, 57198, USA
[2]US Geological Survey (USGS) Earth Resources Observation and Science (EROS) Center, Sioux Falls, SD, 57198, USA

Received: 6 February 2013 – Accepted: 15 February 2013 – Published: 19 March 2013

Correspondence to: G. A. Artan (gartan@usgs.gov)

Published by Copernicus Publications on behalf of the European Geosciences Union.

Abstract

We illustrate the ability to monitor the status of snowpack over large areas by using a spatially distributed snow accumulation and ablation model in the Upper Colorado Basin. The model was forced with precipitation fields from the National Weather Service (NWS) Multi-sensor Precipitation Estimator (MPE) and the Tropical Rainfall Measuring Mission (TRMM) datasets; remaining meteorological model input data was from NOAA's Global Forecast System (GFS) model output fields. The simulated snow water equivalent (SWE) was compared to SWEs from the Snow Data Assimilation System (SNODAS) and SNOwpack TELemetry system (SNOTEL) over a region of the Western United States that covers parts of the Upper Colorado Basin. We also compared the SWE product estimated from the Special Sensor Microwave Imager (SSM/I) and Scanning Multichannel Microwave Radiometer (SMMR) to the SNODAS and SNOTEL SWE datasets. Agreement between the spatial distribution of the simulated SWE with both SNODAS and SNOTEL was high for the two model runs for the entire snow accumulation period. Model-simulated SWEs, both with MPE and TRMM, were significantly correlated spatially on average with the SNODAS ($r = 0.81$ and $r = 0.54$; d.f. = 543) and the SNOTEL SWE ($r = 0.85$ and $r = 0.55$; d.f. = 543), when monthly basinwide simulated average SWE the correlation was also highly significant ($r = 0.95$ and $r = 0.73$; d.f. = 12). The SWE estimated from the passive microwave imagery was not correlated either with the SNODAS SWE or ($r = 0.14$, d.f. = 7) SNOTEL-reported SWE values ($r = 0.08$, d.f. = 7). The agreement between modeled SWE and the SWE recorded by SNODAS and SNOTEL weakened during the snowmelt period due to an underestimation bias of the air temperature that was used as model input forcing.

1 Introduction

Every year large parts of the globe are seasonally covered by snow; for example, every year as much as half of the land surface in the Northern Hemisphere can be snow-covered (Robinson and Kukla, 1985). Most of the water supply for those snow-covered areas comes from snowmelt runoff (Daly et al., 2000; Schmugge et al., 2002; Tekeli et al., 2005); over 60 % of the precipitation in the western United States falls as snow (Serreze et al., 1999). In the Upper Colorado Basin, 63 % of precipitation falls as snow (Fassnacht, 2006), and 70–80 % of total annual runoff comes from snowmelt (Daly et al., 2000; Schmugge et al., 2002). In the past few decades, some basins in the United States have seen historic floods that were induced and triggered from spring rain-on-snow events during years of above average winter snowfall, such as the floods of the Red River of 2009 and 2010. Monitoring the status of snowpack during winter and spring is important to the water resources and disaster management entities.

Several methods have been used to monitor snowpack status: snow course surveys, remote sensing, and snow accumulation/ablation modeling. Worldwide, few areas have reliable ground-observed snowpack status data collected regularly on a large scale, except for the western United States, which is monitored by the SNOwpack TELemetry system (SNOTEL). The representativeness of the snowpack characteristics estimated even from a data-extensive system such as SNOTEL is questioned by some investigators (Daly et al., 2000; Molotch and Bales, 2006).

Because of the limitations of the observational data, several snowpack status monitoring systems that rely on snowmelt models (Pan et al., 2003; Watson et al., 2006) have been described in the literature: snowmelt models combined with remotely sensed data (Cline et al., 1998), remotely sensed data combined with observed snow data (Carroll, 1995; Dressler et al., 2006), and models based solely on remote sensing methods (Bales et al., 2008; Schmugge et al., 2002; Tekeli et al., 2005). A system that utilizes assimilation of data (remotely sensed and insitu measured) and snow accumulation/ablation modeling is the NOAA National Operational Hydrologic Remote Sensing Center (NOHRC; NOHRC, 2004) Snow Data Assimilation System (SNODAS).

Efforts to monitor snowpack status for large areas from remotely sensed data have mainly focused on snow covered area (SCA) mapping (Bales et al., 2008; Kelly et al., 2003; Robinson et al., 1993; Tekeli et al., 2005); however, the snow water equivalent

(SWE) status is what interests water resources and disaster risk managers the most. Despite their coarse spatial resolution and known shortcomings (Kelly et al., 2003), passive microwave sensors like the Scanning Multichannel Microwave Radiometer (SMMR) and the Special Sensor Microwave Imager (SSM/I) have gained some acceptance as tools to map SWE (Chen et al., 2001; Sun et al., 1996).

The objective of this study was to explore the possibility of monitoring the status of the snowpack at regional scales in real time with model and data that are available in even the most data-scarce regions of the globe. The specific aim of our study is to investigate how SWE that is modeled and one that was estimated from passive microwave sensors data compared with SWE values measured by SNOTEL and estimated by SNODAS. In the subsequent sections we will introduce a spatially distributed snow accumulation and ablation model that is forced with remotely sensed data and near-real-time meteorological data from forecast models. We will compare model-simulated SWE with the best available regional SWE datasets. In the comparison, we will include an SWE product estimated from SSM/I and SMMR to substantiate how useful they are in lieu of snowmelt-predicted SWE products.

The snowmelt model we used is a spatially distributed version of the Utah Energy Balance (UEB) model (Tarboton and Luce, 1996). The UEB model has been applied with good results to several basins from different parts the world (Koivusalo and Heikinheimo, 1999; Schulz and de Jong, 2004; Watson et al., 2006). In the subsequent sections, we will describe the model and data, and we will evaluate simulated SWE values over a region of the western United States that covers parts of the Upper Colorado Basin.

2 Study site

Figure 1 depicts the geographic extent of the study area and of the SNOTEL sites that were used in the model verification. The area (43° 48′ N, 116° 6′ W) encompasses a modeling domain of 1 504 800 km^2. The area is rugged and straddles the Continental

HESSD
10, 3629–3664, 2013

Divide and has a mean elevation of 2203 m (σ = 517 m). The SNOTEL sites used for validation are mainly in the Upper Colorado Basin. The average yearly precipitation that falls on the Upper Colorado Basin, estimated from 39 SNOTEL stations, was 700 mm (±184 mm) for the three water years of the study – 2006, 2007, and 2008. The area has a low (~ 11 %) tree vegetation cover.

3 Model and data

SWE recorded from SNODAS and SNOTEL was compared with the SWE simulated by the Utah Energy Balance (UEB) snowmelt model and SWE estimated from microwave imagery. In the following sections, we describe the UEB snowmelt model, model input datasets, and the results of the SWE product intercomparisons. Because the SNODAS system assimilates most of the real-time recorded SWE data in the continental United States, we assumed that the SNODAS SWE data was observed data. Although SNODAS SWE is the best regional scale, spatially distributed SWE data available we are not aware of a comprehensive validation of the SWE estimated by the SNODAS system. The snowmelt model was run for the period December 2005–April 2008.

3.1 Snow accumulation and ablation model

The Utah Energy Balance (UEB) model (Tarboton and Luce, 1996) was used for this work. The UEB model has been applied successfully to diverse basins with good results (Koivusalo and Heikinheimo, 1999; Schulz and de Jong, 2004; Watson et al., 2006). The UEB model solves the snow energy balance at the surface by means of three state variables, snow water equivalence, snow water content, and the age of the snow surface, using a lumped representation of the snowpack as a single layer. Table 1 lists input, output, and model state variables. By using spatially distributed meteorological fields, we assumed that we would able to account for the snow cover heterogeneity component that is due to the variability of the precipitation and solar radiation fields.

For model parameters, we kept the values of the UEB model parameters from Tarboton and Luce (1996) unchanged, except for the snow density, which was changed from 450 kg m^{-3} to 320 kg m^{-3} – value that is more appropriated for the study area (Josberger et al., 1996; Molotch and Bales, 2005). To estimate model parameters, Tarboton and Luce (1996) have a calibration dataset from the Central Sierra Snow Laboratory collected in the winter of 1985–1986. Even though the model has snow redistribution capability, there is no straightforward way to determine appropriate drift factor for every modeling grid. Besides, the sizes of our modeling grids ($0.05 \times 0.05^\circ$ and $0.1 \times 0.1^\circ$) do not warrant modeling snow redistribution processes that usually take place at smaller scales. Therefore, snow redistribution was not taken into account in the simulation results that are presented here.

3.2 Data

The DisUEB model was run with inputs of air temperature, precipitation, wind speed, humidity, and radiation (longwave and shortwave) with temporal resolution of 6-h time steps and spatial resolutions of 0.05×0.05 and 0.1×0.1 degrees (about 5 km and 10 km). Six hours is the maximum time step that is sufficient to resolve the solar diurnal cycle (Tarboton and Luce, 1996). Precipitation is the most important meteorological model input variable. The precipitation data used was from sources: for the 0.05-degree resolution runs the source was the National Weather Service (NWS) regional River Forecast Centers (RFCs) Multi-sensor Precipitation Estimator (MPE) dataset, where the precipitation input for the 0.1-degree resolution runs was the TRMM precipitation estimates. In the subsequent paragraphs, we describe model input meteorological data and the data that was used to test simulated SWE ability to monitor the snowpack water content through the season and Table 1 summarizes the data.

HESSD
10, 3629–3664, 2013

3.2.1 Meteorological Data from Weather Forecast Model

The air temperature (Ta), relative humidity (RH), direct and diffuse solar radiation (Rs), and wind speed (U) were from the NOAA's Global Forecast System (GFS) model. To match the MPE resolution; the Ta, RH, and Rs were downscaled from their original spatial resolution of 0.375-degree resolution grid to a 0.05-degree resolution grid. The downscaling algorithms rely on the topographic data to downscale the coarse weather forecasting model's output fields to the higher resolution. To downscale the three variables terrain geomorphometric characteristics (aspect, slope, and sky-view factor) calculated from a digital elevation model (DEM) were utilized. To redistribute the solar radiation, we used the algorithms of Dozier and Frew (1990) and Dubayah and Van Katwijk (1992). Ta was downscaled with a moist adiabatic lapse rate model (Stone and Carlson, 1979), and RH was downscaled with the re-estimated Ta.

3.2.2 MPE

The MPE data is made by combining data from rain gages, radars, and satellite sensors. The original format of MPE data is in the Hydrologic Rainfall Analysis Project (HRAP) grid format and has an approximate spatial resolution of 4 km. Since the radar coverage of the mountainous areas of the western United States is poor (Wood et al., 2003), especially during the winter, the MPE product west of the Continental Divide is mainly made from gage reports and long-term climatologic precipitation data (PRISM). The MPE has been operational since 2002, but only data from 2005 was available for download from NOAA's Web site at http://water.weather.gov/precip/download.php.

3.2.3 TRMM

The TRMM precipitation data we have used is the 3B42RT product at a 0.25-degree spatial resolution (Tian et al., 2007). The 3B42RT product is made by the combination of precipitation estimates from the TRMM microwave and infrared (IR) sensors. The

HESSD
10, 3629–3664, 2013

microwave sensor provides the main estimates, and the IR sensors provide coverage for areas with gaps in the microwave precipitation estimates. Although the TRMM 3B42 estimates are considered better than the 3B42RT product, the 3B42 is not available in real time as the 3B42RT product is. The 3B42RT products are usually posted to the TRMM Web site about 6 h after the event.

3.2.4 SWE from the microwave imagers

The SWE datasets estimated by microwave imagers that we used are the Global Monthly EASE-Grid SWE Climatology (Armstrong et al., 2007). The EASE-Grid SWE datasets are monthly average values downloaded from the National Snow and Ice Data Center Distributed Active Archive Center (NSIDC, http://nsidc.org/data/), University of Colorado at Boulder. The data is derived from the Scanning Multichannel Microwave Radiometer (SMMR) and selected Special Sensor Microwave/Imagers (SSM/I). The data has a resolution of 25 km, about 0.25 degrees, but since the SSM/I data used to produce the SWE are 19 and 37 GHz (the 19 GHz imagery has a footprint of 69×43 km), the actual resolution of the SWE could be coarser than the nominal 25 km. The microwave-based SWE (MI SWE) spans from December 2005 to April 2007. Only data from December to Aprils was used in the intercomparison with the other SWE products.

3.2.5 SNOTEL

SNOTEL is an automated network of stations that record snow and meteorological variables in the western United States and Alaska. SNOTEL is a Natural Resources Conservation Service (NRCS) network. Most SNOTEL sites are located at higher elevations. We downloaded from the NRCS's Web site (http://www.wcc.nrcs.usda.gov/snow) SWE, precipitation, and air temperature data recorded at 39 stations located in the areas shown in Fig. 1 for the period October 2005–September 2008 and summarized in Table 2.

HESSD
10, 3629–3664, 2013

3.2.6 SNODAS

SNODAS is an NOAA National Operational Hydrologic Remote Sensing Center (NOHRC) SWE dataset (NOHRC, 2004). SNODAS is made by the assimilation of modeled SWE, remotely sensed SWE, and station-recorded SWE data. The SNODAS dataset covers the continental United States at 1-km spatial resolution and 24-h temporal resolution. Although we will consider hereafter the SWE as observed, we are not aware of any extensive validation done on the SNODAS SWE datasets. Because SNODAS assimilates all available observed snow data, it is difficult to validate the accuracy of the SNODAS product. Nevertheless, SNODAS has been used in several research studies and is the only publicly available large-scale SWE product. SNODAS datasets were downloaded from the NSIDC Web site (http://nsidc.org/data). Before comparing SNODAS with other datasets, the SNODAS data were re-gridded to 0.05-, 0.1-, and 0.25-degree resolution from the native 1-km resolution. Table 3 summarizes the spatial and temporal resolutions of the meteorological and snow data that were used in this study.

3.3 Performance indicators

For performance indicators we used the percent of bias, coefficient of determination, total root mean square error (RMSE), and parameters that are based on the RMSE outlined by Willmott (1982). Willmott (1982) decomposed the RMSE into the systematic error (RMSEs), which can be reduced with small improvements in model parameters and input data, and unsystematic RMSE (RMSEu), which cannot be reduced without extensive changes in the model structure and input data. The RMSE, RMSEs, and

Discussion Paper | Discussion Paper | Discussion Paper | Discussion Paper |

HESSD

10, 3629–3664, 2013

Title Page
Abstract Introduction
Conclusions References
Tables Figures
◀| |▶
◀ ▶
Back Close
Full Screen / Esc
Printer-friendly Version
Interactive Discussion

RMSEu parameters are defined (Willmott, 1982) as

$$\mathrm{RMSE} = \left[\frac{1}{n}\sum_{i=1}^{n}(P_i - O_i)^2\right]^{1/2} \tag{1}$$

$$\mathrm{RMSEs} = \left[\frac{1}{n}\sum_{i=1}^{n}\left(\hat{P}_i - O_i\right)^2\right]^{1/2} \tag{2}$$

$$\mathrm{RMSEu} = \left[\frac{1}{n}\sum_{i=1}^{n}\left(\hat{P}_i - P_i\right)^2\right]^{1/2} \tag{3}$$

where n is the number of observations, O_i is the observed value, P_i is the predicted value, and $\hat{P}_i = a \cdot O_i + b$. To describe how much the model underestimates or overestimates the variable of interest, the percent bias was calculated according to

$$\mathrm{Bias} = 100 \times \frac{\sum_{i=1}^{n} P_i - \sum_{i=1}^{n} O_i}{\sum_{i=1}^{n} O_i} \tag{4}$$

4 Results and discussion

4.1 Snowmelt model meteorological inputs

We tested the precipitation reported by MPE and TRMM by comparing to precipitation value recorded at the 39 SNOTEL stations shown in Fig. 1. By comparing gridded data of varying spatial scales and point data there should not be an expectation of perfect agreement even if both data are correct. We compared precipitation totals accumulated in the snow accumulation/ablation periods of the three years of the simulation period –

1 January 2006–30 April 2006, 1 January 2007–30 April 2007, and 1 January 2008–28 April 2008 (d.f. = 115). Both MPE and TRMM were negatively biased against SNOTEL precipitation as illustrated in Fig. 2; on average the percent bias of the MPE per season for the 39 locations was −26 % with mean and standard deviation of -84 ± 110 mm, where for the TRMM the bias was −51 % (-164 ± 124 mm). The correlation between the MPE and TRMM was even lower than the one the two datasets had with SNOTEL data ($r = 0.53$). Higher proportions of the precipitation differences with SNOTEL sets were systematic errors for both the TRMM (86 % of RMSE) and the MPE datasets (77 % of RMSE). The higher systematic errors of the TRMM and MPE data means that the data could be improved with simpler correction schemes.

The large discrepancy of the MPE compared with SNOTEL is difficult to explain even when the perils of comparing gridded precipitation with values from a single gage are taken into account. The discrepancies could be due to the difference between the methods used to calculate the MPE values east and west of the Continental Divide. The large magnitude of the discrepancy between some of the SNOTEL station-recorded precipitation and the MPE suggests that there is a need to improve the MPE estimation. Our results on the bias direction, being inclined for underestimation, are in line with what Habib et al. (2009) observed when they weighted precipitation values from MPE against raingage-recorded precipitation.

The GFS daily mean Ta extracted from grid-cells was compared to SNOTEL-recorded Ta the 39 stations, which were described in the preceding sections. The GFS's Ta was created by averaging four 6-hourly Ta. The comparison period was same as the precipitation evaluation period – winter and spring, when the Ta influences the snow process. The 39 sites elevation ranges from 2268 m to 3487 m. Figure 3 shows the plots of the average daily GFS- and SNOTEL-recorded Ta for the 39 sites for the three seasons. GFS's Ta matches the seasonally of the SNOTEL recorded Ta (Fig. 3). The Ta of both GFS and SNOTEL were significantly correlated ($R^2 = 0.61$, d.f. = 171), but the GFS's Ta were negatively biased versus the Ta recorded at the SNOTEL sites (Fig. 4). The bias, between GFS and SNOTEL Ta, was not correlated with elevation

HESSD
10, 3629–3664, 2013

(Fig. 5). The negative bias of the GFS's Ta is counterintuitive given that usually the SNOTEL sites are located at higher elevations than the surrounding terrain. The presence of a negative bias within all elevation bands suggests that the elevation correction applied to the original GFS data was not the cause of the biases but rather a systematic GFS's underestimation bias. Others have reported similar results of negative biases of weather forecast model air temperature in the western United States during the winter months (Pan et al., 2003).

4.2 Spatial intercomparisons of the SWE datasets

The SWE grids simulated with the UEB model and the SWE grids estimated from MI were compared against SWE from SNOTEL and SNODAS. While the SWE from the UEB simulation and SNODAS system had only a few grids with missing data (grids over water bodies), the SWE estimated from the MI datasets has a high number of pixels with missing data. For example, MI-estimated SWE had missing data in 40 % of the area for February 2007 (Fig. 6). The evaluation of the SWE was done at the grids corresponding with the sites of the 39 SNOTEL sites shown in Fig. 1. The SNODAS grids used in the comparisons were upscaled from their native 1-km (∼ 0.01-degree) resolution to grids with 0.05-, 0.10-, and 0.025-degree resolution. Statistical indexes (correlation coefficients, percent biases, RMSE, RMSEs, and RMSEu) were calculated at each of the 39 validation sites between the SNODAS SWE and MI- and UEB-produced SWE. Additionally, to give a contextual frame-of-reference, the SWE products were compared to the SWE recorded at the 39 sites by SNOTEL system.

The average monthly SWE value recorded at the SNOTEL sites was 259 ± 96 mm (mean ± standard deviation) and 240 ± 98 mm for the periods January 2006–April 2008 (UEB simulations period) and January 2006–April 2007 (the period where MI-estimated SWE were available), respectively. Of the 39 sites the SWE products simulated with the UEB were significantly correlated with the SNODAS SWE ($p = 0.05$) in 37 and 23 sites for the MPE and TRMM precipitation, respectively (Fig. 7a). The SWE estimated from MI was not significantly correlated ($p = 0.05$) with the SNODAS SWE at 28 sites

HESSD
10, 3629–3664, 2013

(Fig. 7a). The correlation between the SWE products and the SNOTEL recorded SWE was significant at 37, 23, and 12 sites for the UEB-MPE, and UEB-TRMM, and MI-SWE products, respectively (Fig. 7b).

Figure 8a–f shows linear and box plots of the three SWE products contrasted with concurrent SNOTEL and SNODAS SWE. The MI-estimated SWE consistently underestimates the SWE depicted by the SNODAS or the SNOTEL (Fig. 8c). The SWE simulated with the UEB model forced with TRMM data for precipitation also consistently underpredicted the SWE most of the time (Fig. 8b). The SWE modeled with UEB driven with the MPE data was in good agreement with the SNODAS and SNOTEL SWE values, except for one location that had an extremely large SWE value (Fig. 8d).

Given the large difference in precipitation and elevation between the sites, it is fair to expect that SWE would vary greatly between sites. Accumulated precipitation recorded by the SNOTEL network at 39 sites for the snow melt/accumulation months of 2006–2008 ranged from 109 mm to 826 mm. The SWE simulated with the TRMM precipitation (Fig. 8e) and MI-estimated SWE had a much narrower interquartile range than the SWE simulated with MPE (Fig. 8f). The process of upscaling by itself narrows the interquartile range as shown by the SNODAS data (Fig. 8d, f). Although small the variability seen in Figures 8d the TRMM does not lacks the ability to differentiate sites with high snowfall from sites with small snowpack given the statistically significant correlation it has with SNODAS and SNOTEL SWE in more than half of the sites. We think that the lower variability of the TRMM-simulated SWE were in part due to the model grid resolution being sub-optimal to modeling the snow accumulation/ablation processes in the study area (Artan et al., 2000; Blöschl, 1999).

Tables 4 and 5 summarize the statistical indices of the SWE comparisons. Of the three SWE products, the SWE simulated with UEB when forced with NOAA's MPE precipitation was the best performer. The SWE TRMM-simulated SWE and MI-estimated are not adept as site specific snowpack monitoring tools.

Figure 9a–f shows the relationship between the elevation and the correlations the SNODAS estimated SWE has with the SWE predicted from the UEB or the SWE estimated from the MI imagery. The MI-estimated SWE products have a significant negative correlation ($r = -0.45$, d.f. $= 37$, $p < 0.05$) with the elevation value of the sites, but neither of the two SWE simulated with UEB exhibited any relationship with elevation (Fig. 9b, c). The MI provides better prediction of SWE at lower elevation terrains. All three SWE products had the lowest skills in the southwest of the study area.

Among the three SWE datasets we evaluated to reproduce SWE values seen in the SNODAS and SNOTEL datasets, the performance of the MI-estimated SWE was the worst in most of the correlation metrics. The MI SWE had the lowest correlation with the SNODAS and SNOTEL SWE. Both, MI estimated and UEB-TRMM simulated, SWE had a relatively large systematic errors. Also, the skills of the MI-estimated SWE to reproduce the values recorded by SNOTEL and SNODAS were negatively correlated with the elevation. Other researchers have also reached similar conclusions on the poor performance of MI-estimated SWE for the mountainous western United States; for example, Dong et al. (2005) found that in the western United States, the complex nature of the terrain and climate causes a significant error in the estimation of SWE from microwave imagery. The low random error component, once the source of the errors are fully know, should make possible the improvement of the UEB-TRMM and Mi-estimated SWE product.

4.3 Temporal intercomparisons of the SWE datasets

The average SWE value at the 39 SNOTEL sites was calculated at every time step (14 month of data for all products except the MI-estimated SWE only 9 months of data were available) for the simulated or observed SWE datasets. Figure 10a–c shows the time series plots of the evolution through the season of the average SWE in the study area from SNOTEL, SNODAS, estimated from MI, and simulated by the UEB. All of the SWE products displayed a similar evaluation of the SWE temporal pattern. The SWE estimated from the MI showed (Fig. 10a) an earlier start of the melt season than either SNODAS or SNOTEL, but the snowpack simulated with the UEB model (Fig. 10b, c) started the melt season about 10 days later than SNODAS. Although the

SWE estimated from the MI has a monthly time step that makes it difficult to quantify accurately the exact date of the start of the melt season, prediction of the start of the melt season of one month earlier by the MI will decrease the usefulness of the SWE-MI product for monitoring purposes. The SNODAS SWE start of the melt period for two seasons (2006/2007 and 2007/2008) was about one week earlier than SNOTEL's.

Figure 11a–d presents the linear relationships between the average monthly values of the SWE products. The SWE estimated from the MI was not significantly correlated with the SNODAS SWE (Fig. 11a). But the SWE simulated with the UEB models was in good agreement with the SNODAS-estimated SWE (Fig. 11b, c) with a clear linear relationship. The UEB-simulated SWE mostly captured the SNODAS SWE evolution through the season, and the only major diverges noticeable from the linear line is during the period of rapid melts. During such a period, the SNODAS SWE trends lower, where the SWE simulated with UEB was still in the snow accumulation period. The later start of the melt season seen in the plots of UEB-simulated SWE (Fig. 10b, c and Fig. 11b, c) was due to the negative bias seen in model input air temperature (Fig. 4) and elucidates the effects of the errors in the input meteorological data on the UEB-simulated SWE. Figure 11d shows the average area-wide SWE from the SNODAS and SNOTEL datasets. The striking feature of Fig. 11d is the great agreement between the two products in the three years of the comparison (14 months).

For most of the time, the UEB model underestimated SWE compared to the SWE values recorded at the SNOTEL stations and SNODAS. Our findings, on the underestimation of the simulated SWE, are consistent with the findings of other research on the underestimation biases of simulated SWE in the mountainous western United States (Pan et al., 2003). The underestimation of the simulated SWE was consistent with the negative biases that MPE and TRMM precipitation datasets had when contrasted with SNOTEL precipitation recorded at a location inside the MPE or TRMM grid. Overall, the UEB-simulated SWE showed remarkable predictive skills compared to the SWE predicted by the SNODAS, and the agreement between the SNODAS- and SNOTEL-recorded SWE was marginal. Although the TRMM simulated SWE had low quantitative

HESSD
10, 3629–3664, 2013

skills to predict snow water content nevertheless had good qualitative skills to predict snow water given the high correlation it exhibited when compared with SNODAS data.

From a practical point-of-view, we found the MI-estimated SWE to be unreliable sources for mapping SWE in the study area and to have a large underestimation bias compared with the SNOTEL SWE or the SWE estimated by the SNODAS system. Our results on the negative biases of the MI-estimated SWE are different from what Mote et al. (2003) reported. Mote et al. (2003) found that SWE estimated from SSM/I overpredicted during the melting period for five sites in the northern Great Plains.

5 Conclusions

We presented a distributed snow accumulation and ablation model; build on the UEB model, that uses data from weather forecast models as forcing input. Besides the weather forecast model (GFS) data, the snowmelt model was forced with two precipitation datasets: the NWS's MPE and the TRMM precipitation estimates. The model was run at a 0.050- and 0.100-degree resolution for the MPE and TRMM, respectively. We compared model-simulated SWE and MI-estimated SWE with co-located SWE datasets recorded by the SNOTEL network or estimated by the SNODAS system. The SWE simulated by the UEB model was strongly correlated with the SWE estimated by SNODAS ($R^2 = 0.54$ and $R^2 = 0.90$ for model input precipitation as TRMM and MPE, respectively) and the SWE recorded by SNOTEL ($R^2 = 0.40$ and $R^2 = 0.81$) when the seasonal average SWE values were compared. The MI-estimated SWE was not significantly correlated with either of the SNOTEL or SNODAS SWE products (R^2 of 0.0 and 0.02, respectively).

Both of the UEB-simulated and MI-estimated SWEs underestimated the SWE reported by the SNOTEL or SNODAS systems but were found to be useful in mapping the SWE. The MI-estimated SWE underestimated the SWE values seen in the SNOTEL and SNODAS datasets and lacked a discernable variability between sites seen in the SNOTEL and SNODAS SWE data and were found to be unreliable sources for

HESSD
10, 3629–3664, 2013

mapping SWE in the study area. In the future, we will evaluate the effects of the parameterization of the snow albedo on the snowmelt processes by using remotely sensed snow albedo as input to the model. Notwithstanding their experimental nature, several snow albedo products with near-global coverage are now becoming available.

References

Armstrong, R. L. and Brodzik, M. J.: Recent Northern Hemisphere snow extent: a comparison of data derived from visible and microwave satellite sensors, Geophys. Res. Lett., 28, 3673–3676, 2001.

Armstrong, R. L., Brodzik, M. J., Knowles, K., and Savoie, M.: Global monthly EASE-Grid snow water equivalent climatology, National Snow and Ice Data Center, Digital Media, Boulder, CO, 2007.

Artan, G. A., Neale, C. M. U., and Tarboton, D. G.: Characteristic length scale of input data in distributed models: implications for modeling grid size, J. Hydrol., 227, 128–139, 2000.

Bales, R. C. and Harrington, R. F.: Recent progress in snow hydrology, Rev. Geophys., 33, 1011–1020, 1995.

Bales, R. C., Dressler, K. A., Imam, B., Fassnacht, S. R., and Lampkin, D.: Fractional snow cover in the Colorado and Rio Grande basins, 1995–2002, Water Resour. Res., 44, W01425, doi:10.1029/2006WR005377, 2008.

Blöschl, G.: Scaling issues in snow hydrology, Hydrol. Process., 13, 2149–2175, 1999.

Bloschl, G., Kirnbauer, R., and Gutknecht, D.: Distributed snowmelt simulations in an alpine catchment. I. Model evaluation on the basis of snow cover patterns, Water Resour. Res., 27, 3171–3179, 1991.

Carroll, S. S.: Modeling measurement errors when estimating snow water equivalent, J. Hydrol., 172, 247–260, 1995.

Chen, C.-T., Nijssen, B., Guo, J., Tsang, L., Wood, A. W., Hwang, J.-N., and Lettenmaier, D. P.: Passive microwave remote sensing of snow constrained by hydrological simulations, IEEE T. Geosci. Remote, 39, 1744–1756, 2001.

Cline, D. W.: Snow surface energy exchanges and snowmelt at a continental, midlatitude Alpine site, Water Resour. Res., 33, 689–701, 1997.

Cline, D. W., Bales, R. C., and Dozier, J.: Estimating the spatial distribution of snow in mountain basins using remote sensing and energy balance modeling, Water Resour. Res., 34, 1275–1285, 1998.
Daly, S. F., Davis, R., Ochs, E., and Pangburn, T.: An approach to spatially distrubuted snow modelling of the sacramento and San Joaquin basins, California, Hydrol. Process., 14, 3257–3271, 2000.
Dong, J., Walker, J. P., and Houser, P. R.: Factors affecting remotely sensed snow water equivalent uncertainty, Remote Sens. Environ., 97, 68–82, 2005.
Dozier, J. and Frew, J.: Rapid calculation of terrain parameters for radiation modeling from digital elevation data, IEEE T. Geosci. Remote Sens., 28, 963–969, 1990.
Dressler, K. A., Leavesley, G. H., Bales, R. C., and Fassnacht, S. R.: Evaluation of gridded snow water equivalent and satellite snow cover products for mountain basins in a hydrologic model, Hydrol. Process., 20, 673–688, 2006.
Dubayah, R. and Van Katwijk, V.: The topographic distribution of annual incoming solar radiation in the Rio Grande River Basin, Geophys. Res. Lett., 19, 2231–2234, 1992.
Fassnacht, S. R.: Upper versus lower Colorado River sub-basin streamflow: characteristics, runoff estimation and model simulation, Hydrol. Process., 20, 2187–2205, 2006.
Fierz, C., Riber, P., Adams, E. E., Curran, A. R., Föhn, P. M. B., Lehning, M., and Plüss, C.: Evaluation of snow-surface energy balance models in alpine terrain, J. Hydrol., 282, 76–94, 2003.
Garen, D. C. and Marks, D.: Spatially distributed energy balance snowmelt modelling in a mountainous river basin: estimation of meteorological inputs and verification of model results, J. Hydrol., 315, 126–153, 2005.
Habib, E., Larson, B. F., and Graschel, J.: Validation of NEXRAD multisensor precipitation estimates using an experimental dense rain gauge network in south Louisiana, J. Hydrol., 373, 463–478, 2009.
Janowiak, J. E., Joyce, R. J., and Yarosh, Y.: A real-time global half-hourly pixel-resolution infrared dataset and its applications, B. Am. Meteorol. Soc., 82, 205–217, 2001.
Josberger, E. G., Gloersen, P., Chang, A., and Rango, A.: The effects of snowpack grain size on satellite passive microwave observations from the Upper Colorado River Basin, J. Geophys. Res. C: Oceans, 101, 6679–6688, 1996.

Joyce, R. J., Janowiak, J. E., Arkin, P. A., and Xie, P.: CMORPH: A method that produces global precipitation estimates from passive microwave and infrared data at high spatial and temporal resolution, J. Hydrometeorol., 5, 487–503, 2004.

Kelly, R. E., Chang, A. T., Tsang, L., and Foster, J. L.: A prototype AMSR-E global snow area and snow depth algorithm, IEEE T. Geosci. Remote, 41, 230–242, 2003.

Koivusalo, H. and Heikinheimo, M.: Surface energy exchange over a boreal snowpack: comparison of two snow energy balance models, Hydrol. Process., 13, 2395–2408, 1999.

Letsinger, S. L. and Olyphant, G. A.: Distributed energy-balance modeling of snow-cover evolution and melt in rugged terrain: Tobacco Root Mountains, Montana, USA, J. Hydrol., 336, 48–60, 2007.

Marks, D., Domingo, J., Susong, D., Link, T., and Garen, D.: A spatially distributed energy balance snowmelt model for application in mountain basins, Hydrol. Process., 13, 1935–1959, 1999.

Molotch, N. P. and Bales, R. C.: Scaling snow observations from the point to the grid element: implications for observation network design, Water Resour. Res., 41, 1–16, 2005.

Molotch, N. P. and Bales, R. C.: SNOTEL representativeness in the Rio Grande headwaters on the basis of physiographics and remotely sensed snow cover persistence, Hydrol. Process., 20, 723–739, 2006.

Mote, T. L., Grandstein, A. J., Leathers, D. J., and Robinson, D. A.: A comparison of modeled, remotely sensed, and measured snow water equivalent in the northern Great Plains, Water Resour. Res., 39, 1209, doi:10.1029/2002WR001782, 2003.

Ming, P., Sheffield, J., Wood, E. F., Mitchell, K. E., Houser, P. R., Schaake, J. C., Robock, A., Lohmann, D., Cosgrove, B., Duan, Q., Luo, L., Higgins, R. W., Pinker, R. T., and Tarpley, J. D.: Snow process modeling in the North American Land Data Assimilation System (NLDAS): 1. evaluation of model simulated snow water equivalent, J. Geophys. Res. D: Atmos., 108, 8850, doi:10.1029/2003JD003994, 2003.

Robinson, D. A. and Kukla, G.: Maximum surface albedo of seasonally snow-covered lands in the Northern Hemisphere, J. Climate Appl. Meteorol., 24, 402–411, 1985.

Robinson, D. A., Dewey, K. F., and Heim Jr., R. R.: Global snow cover monitoring: an update, B. Am. Meteorol. Soc., 74, 1689–1696, 1993.

Schmugge, T. J., Kustas, W. P., Ritchie, J. C., Jackson, T. J., and Rango, A.: Remote sensing in hydrology, Adv. Water Resour., 25, 1367–1385, 2002.

Schulz, O. and de Jong, C.: Snowmelt and sublimation: field experiments and modelling in the High Atlas Mountains of Morocco, Hydrol. Earth Syst. Sci., 8, 1076–1089, doi:10.5194/hess-8-1076-2004, 2004.

Serreze, M. C., Clark, M. P., Armstrong, R. L., McGinnis, D. A., and Pulwarty, R. S.: Characteristics of the western United States snowpack from snowpack telemetry (SNOTEL) data, Water Resour. Res., 35, 2145–2160, 1999.

Sun, C., Neale, C. M. U., and McDonnell, J. J.: Snow wetness estimates of vegetated terrain from satellite passive microwave data, Hydrol. Process., 10, 1619–1628, 1996.

Tarboton, D. G. and Luce, C. H.: Utah Energy Balance Snow Accumulation and Melt Model (UEB): Computer model technical description and users guide, Utah Water Research Laboratory and USDA Forest Service Intermountain Research Station, Logan, Utah, 64 pp., 1996.

Tekeli, A. E., Akyürek, Z., Şorman, A. A., Şensoy, A., and Şorman, A.Ü.: Using MODIS snow cover maps in modeling snowmelt runoff process in the eastern part of Turkey, Remote Sens. Environ., 97, 216–230, 2005.

Tian, Y., Peters-Lidard, C., Choudhury, B., and Garcia, M.: Multitemporal analysis of TRMM-based satellite precipitation products for land data assimilation applications, J. Hydrometeorol., 8, 1165–1183, 2007.

Watson, F. G. R., Newman, W. B., Coughlan, J. C., and Garrott, R. A.: Testing a distributed snowpack simulation model against spatial observations, J. Hydrol., 328, 453–466, 2006.

Willmott, C. J.: Some comments on the evaluation of model performance, B. Am. Meteorol. Soc., 63, 1309–1313, 1982.

Wood, V. T., Brown, R. A., and Vasiloff, S. V.: Improved detection using negative elevation angles for mountaintop WSR-88Ds. Part II: Simulations of the three radars covering Utah, Weather Forecast., 18, 393–403, 2003.

Xie, P. and Arkin, P. A.: Global precipitation: a 17-year monthly analysis based on gauge observations, satellite estimates, and numerical model outputs, B. Am. Meteorol. Soc., 78, 2539–2558, 1997.

HESSD

10, 3629–3664, 2013

Large scale snow water status monitoring

G. A. Artan et al.

HESSD
10, 3629–3664, 2013

Large scale snow water status monitoring

G. A. Artan et al.

Table 1. Snowmelt model inputs, outputs, and state variables. The input includes static distributed parameters and dynamic meteorological data.

Dynamic inputs	Static inputs	Output fluxes	State variables
Incoming shortwave rad.	Elevation	Latent heat flux	Snow energy content
Incoming longwave rad.	Vegetation cover	Sensible heat flux	Snow water content
Air temperature	Vegetation height	Ground heat flux	Snow age
Average wind speed	Soil bulk density	Snow temperature	
Precipitation		Melt advected energy	
Relative humidity		Melt outflow flux	
Atmospheric pressure			

Table 2. Locations of the SNOTEL station where simulated SWE and MI-estimated SWE were validated.

Station ID	Station Name	Lat	Long	Elevation
1	Brumley	39.08	−106.53	3231
2	Columbine Pass	38.42	−108.37	2865
3	Elk River	40.83	−106.97	2652
4	Lost Dog	40.80	−106.73	2841
5	Mccoy Park	39.60	−106.53	2890
6	Middle Fork Camp	39.78	−106.02	2725
7	Park Cone	39.82	−106.58	2926
8	Park Reservoir	39.03	−107.87	3036
9	Lone Cone	37.88	−108.18	2926
10	Elkhart Park	43.00	−109.75	2865
11	Battle Mountain	41.03	−107.25	2268
12	New Fork Lake	43.12	−109.93	2542
13	East Rim Divide	43.13	−110.20	2417
14	Sandstone Rs	41.12	−107.17	2484
15	Hickerson Park	40.90	−109.95	2787
16	Trout Creek	40.73	−109.67	2901
17	Mosby Mtn	40.60	−109.88	2899
18	Lakefork #1	40.58	−110.43	3174
19	Loomis Park	43.17	−110.13	2512
20	Snider Basin	42.48	−110.52	2457
21	Bison Lake	39.75	−107.35	3316
22	Burro Mountain	39.87	−107.58	2865
23	Hams Fork	42.15	−110.67	2390
24	King's Cabin	40.70	−109.53	2659
25	Idarado	37.93	−107.67	2987
26	Porphyry Creek	38.48	−106.33	3280
27	Slumgullion	37.98	−107.20	3487
28	Butte	38.88	−106.95	3097
29	Dry Lake	40.53	−106.77	2560
30	Gunsight Pass	43.37	−109.87	2993
31	Kendall R.S.	43.23	−110.02	2359
32	Stillwater Creek	40.22	−105.92	2658
33	Rock Creek	40.53	−110.68	2405
34	Indian Creek	42.30	−110.67	2873
35	Lizard Head Pass	37.78	−107.92	3109
36	Spring Creek Divide	42.52	−110.65	2743
37	El Diente Peak	37.78	−108.02	3048
38	Townsend Creek	42.68	−108.88	2652
39	McClure Pass	39.12	−107.28	2896

HESSD
10, 3629–3664, 2013

Large scale snow water status monitoring

G. A. Artan et al.

Table 3. Source and resolution of meteorological and snow data.

Data	Source	Resolution		Downscaling
		Spatial	Temporal	
Ta, RH, Rs, U	NOAA's GFS Model	$0.375 \times 0.375^{\circ}$	6-h	0.05-, 0.1-degrees
MPE	NWS RFCs	4×4 km	24-h	0.05-, 0.1-degrees
TRMM	NASA	$0.25 \times 0.25^{\circ}$	3-h	0.1-degrees
SWE (EASE-Grid)	NSIDC	$0.25 \times 0.25^{\circ}$	24-h	none
SWE, Ta	SNOTEL	Point data	24-h	none
SWE (SNODAS)	NOAA NOHRC	1×1 km	24-h	0.05-degrees

HESSD
10, 3629–3664, 2013

Table 4. Statistical summary of the comparison between the SWE products and the SNOTEL datasets. The last row is the statistics summery of comparison between the 0.05-degree resolution SNODAS and the point SNOTEL SWE.

Dataset	Mean $\pm\sigma$	r^2	Bias	RMSE	RMSEs	RMSEu
Microwave	60 ± 22	0.01	−77	223	222	21
UEB-TRMM	59 ± 18	0.30	−77	225	224	18
UEB-MPE	155 ± 64	0.72	−40	121	115	39
SNODAS	217 ± 95	0.84	−16	69	46	52

Table 5. Statistical summary of the evaluation of SWE products compared to the SNODAS product. The SNODAS product compared to each product had the spatial and temporal resolution as the products (0.05-, 0.10-, and 0.25-degree resolution; daily or monthly).

Dataset	Mean $\pm\sigma$	r^2	Bias	RMSE	RMSEs	RMSEu
Microwave	60 ± 22	0.08	−64	151	149	20
UEB-TRMM	59 ± 18	0.29	−71	181	179	29
UEB-MPE	155 ± 64	0.65	−28	88	78	41

HESSD
10, 3629–3664, 2013

Large scale snow water status monitoring

G. A. Artan et al.

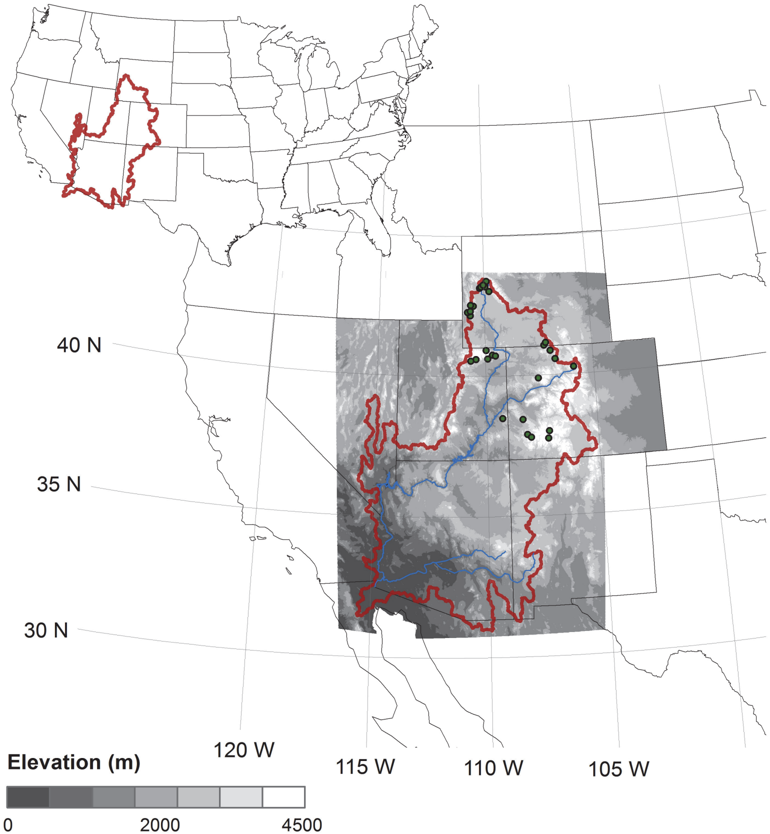

Fig. 1. A shaded relief map of the study area and locations of the SNOTEL sites with an outline of the Colorado Basin and western US States.

HESSD
10, 3629–3664, 2013

Large scale snow water status monitoring

G. A. Artan et al.

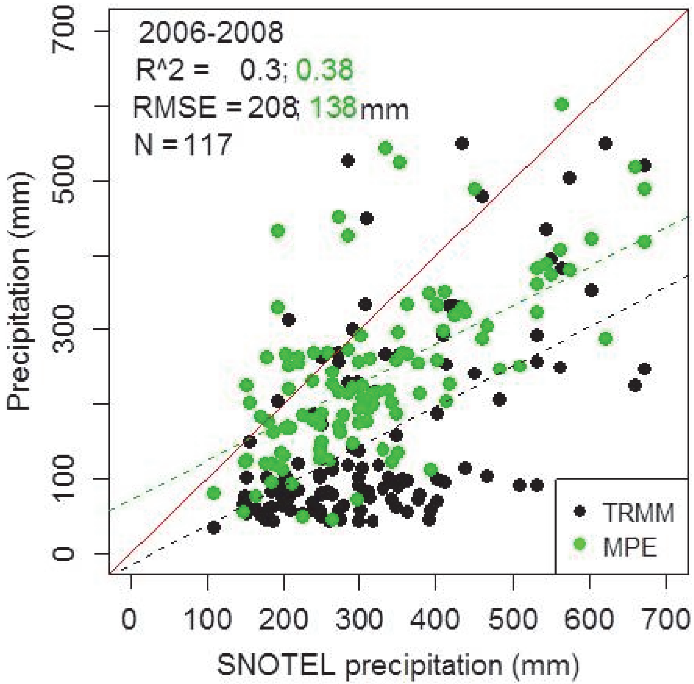

Fig. 2. Scatterplots of the total precipitation recorded at 39 SNOTEL sites for the periods of 1 January 2006–30 April 2006, 1 January 2007–30 April 2007, and 1 January 2008–28 April 2008 compared with precipitation estimates for the same locations from MPE (black) and TRMM (green).

HESSD
10, 3629–3664, 2013

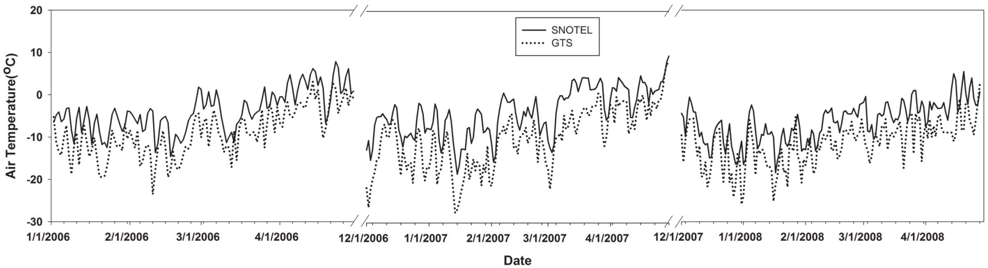

Fig. 3. Average daily forecasted GFS air temperature (dotted) and SNOTEL-recorded daily average temperature (solid line) at the 39 SNOTEL sites. GFS's air temperatures were extracted from 0.05-degree resolution grids and an average of the 06:00 Z, 12:00 Z, 18:00 Z, and the following day 00:00 Z forecasts.

HESSD
10, 3629–3664, 2013

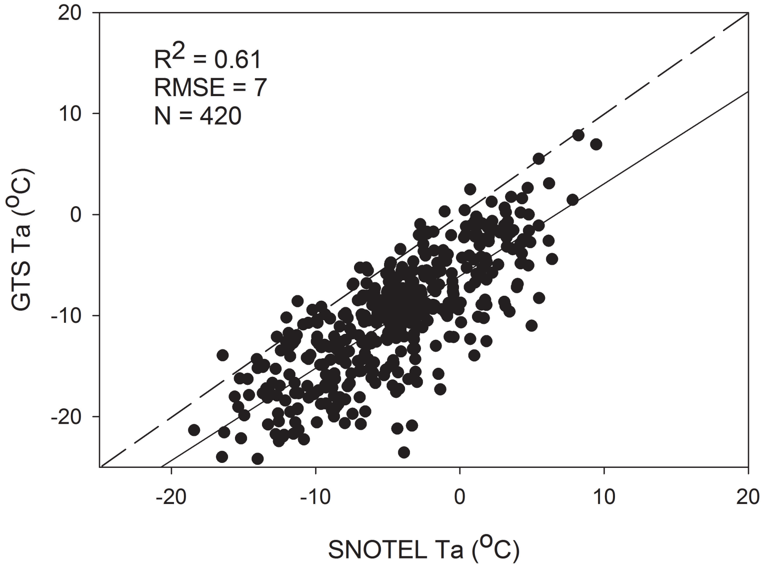

Fig. 4. Scatterplots of the averages of daily air temperature at 39 SNOTEL from the GFS and SNOTEL.

HESSD
10, 3629–3664, 2013

Large scale snow water status monitoring

G. A. Artan et al.

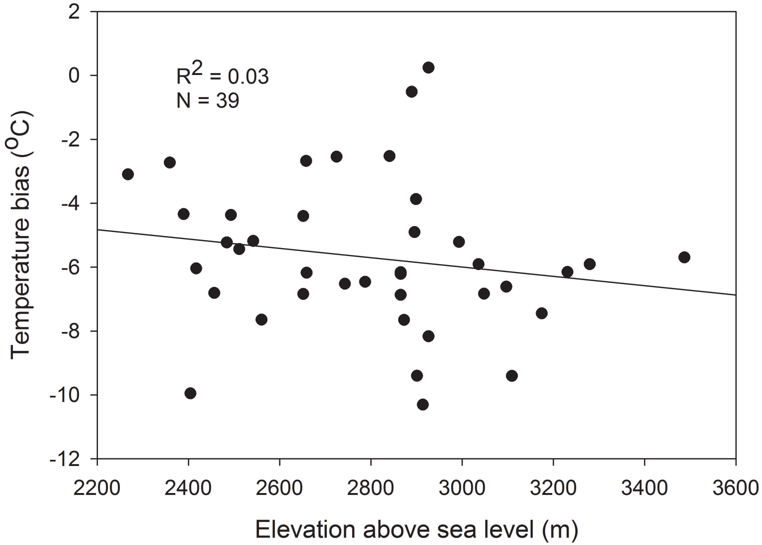

Fig. 5. Bias of the GFS average daily air temperature from the air temperature recorded at the SNOTEL sites and sites elevation.

HESSD
10, 3629–3664, 2013

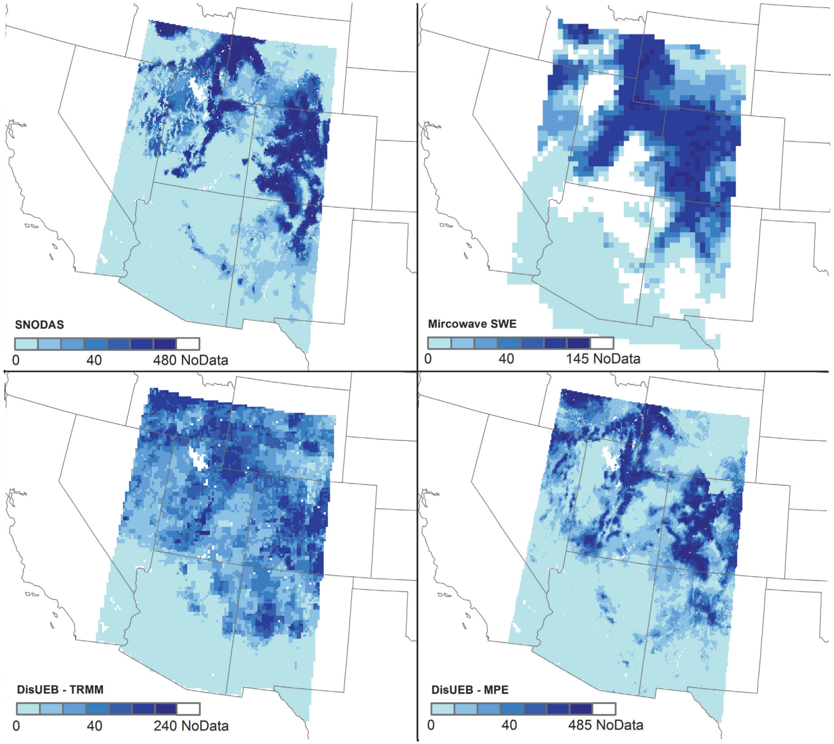

Fig. 6. Average SWE for February 2007 predicted with distributed UEB model and microwave imagery, and SNODAS. Over 40 % of the area had missing data for SWE dataset estimates from the microwave imagery.

HESSD
10, 3629–3664, 2013

Large scale snow water status monitoring

G. A. Artan et al.

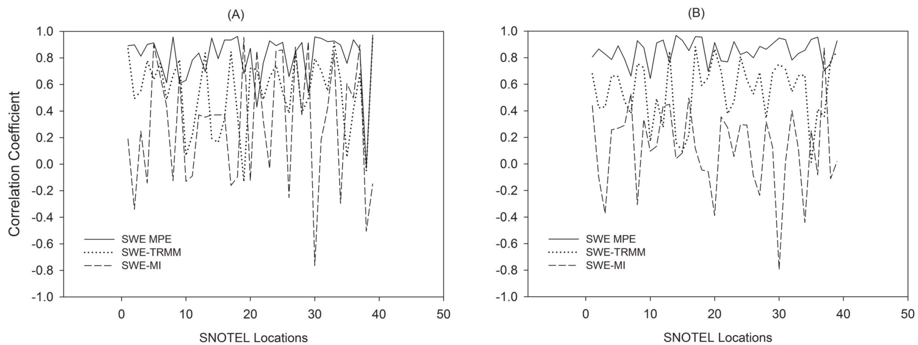

Fig. 7. Correlation coefficients between the average seasonal **(A)** SNODAS SWE at various grid resolutions and **(B)** the SWE recorded by the SNOTEL site at 39 sites in the upper Colorado Basin with the SWE estimates products from the MI imagery and UEB simulations.

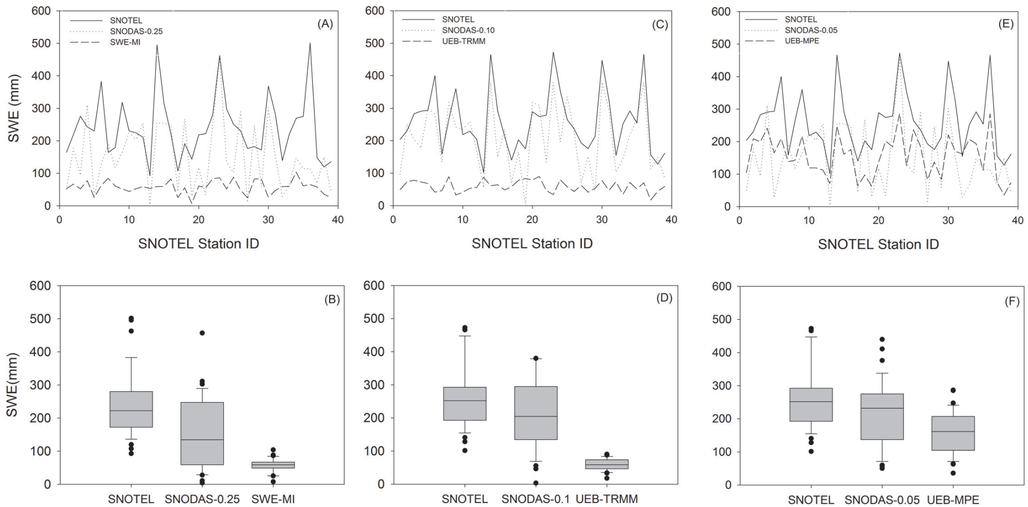

Fig. 8. Average SWE from SNOTEL and SNODAS for the winter and spring months compared with SWE estimated from **(A)** MI, **(C)** SWE predicted with UEB when driven with TRMM precipitation, and **(E)** UEB forced with MPE precipitation. The SWE simulated with the UEB is for the period November 2006–April 2008, excluding the months from June to October. **(B, D, F)** are box-plots of the data in the first three graphs.

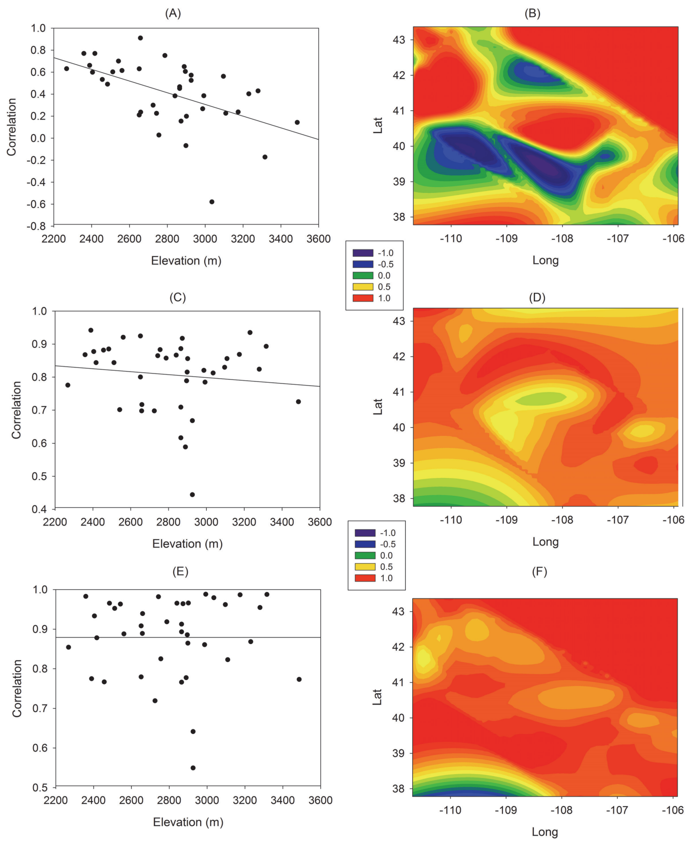

Fig. 9. Relationships between elevations and correlation between the SWE of SNODAS, and spatial distribution of the correlation coefficients plotted at the SNOTEL sites and **(A–B)** the SWE estimated from microwave imagers, **(C–D)** SWE simulated with UEB forced with TRMM precipitation data, and **(E–F)** simulated with the UEB with MPE as input precipitation dataset.

HESSD
10, 3629–3664, 2013

Large scale snow water status monitoring

G. A. Artan et al.

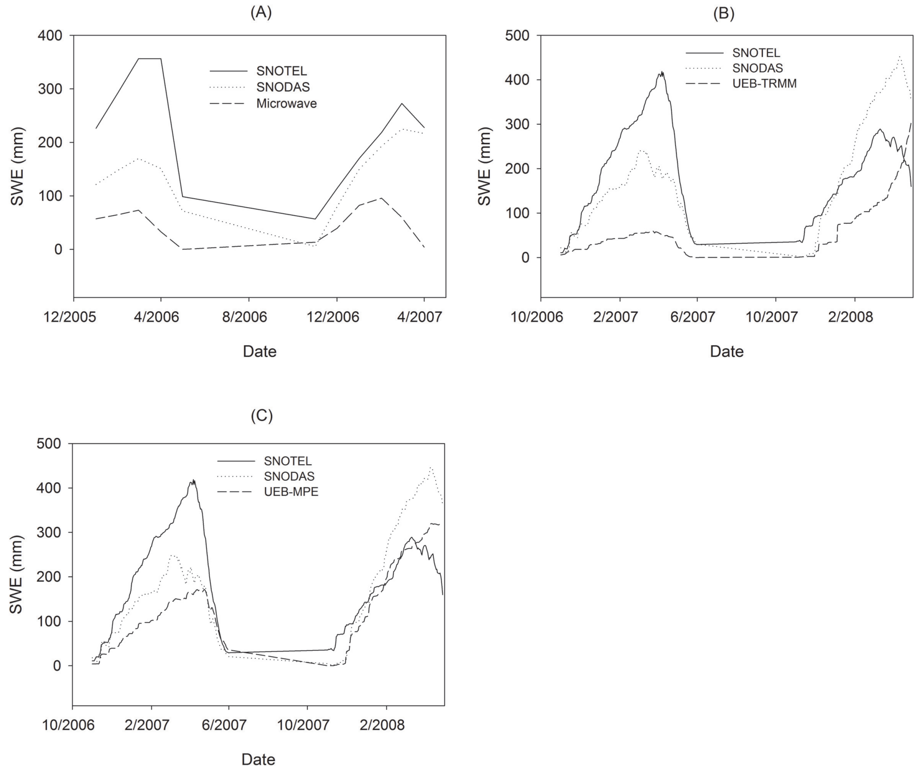

Fig. 10. Time series plots of averaged SWE (at the 39 SNOTEL sites) from SNOTEL and SNODAS and **(A)** the microwave imagers, **(B)** simulated with the UEB model with TRMM precipitation, and **(C)** modeled with UEB model and MPE precipitation.

HESSD
10, 3629–3664, 2013

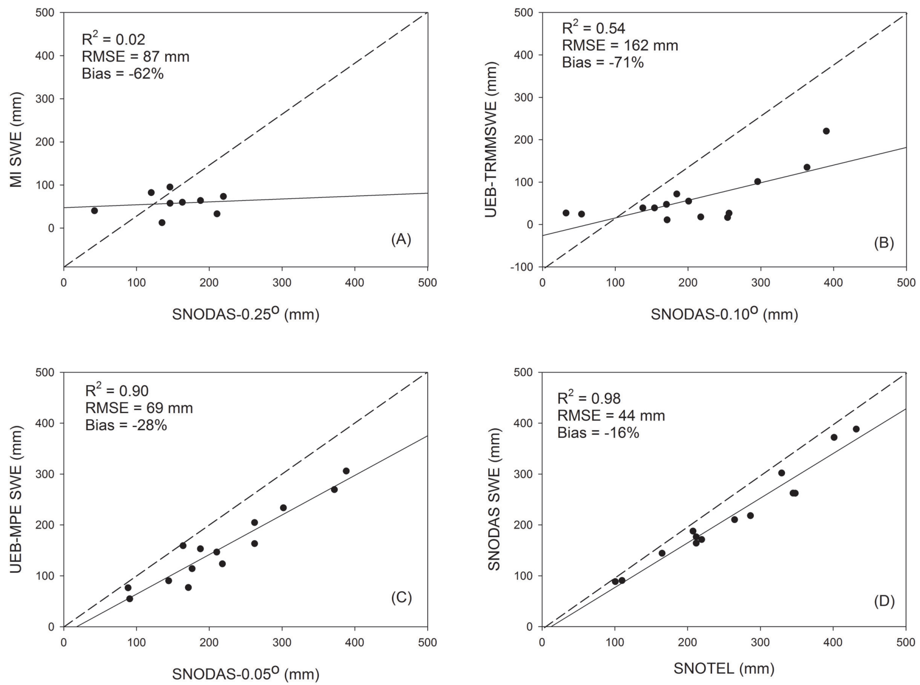

Fig. 11. Averaged SWE (at the 39 SNOTEL sites) from the SNODAS and the **(A)** SWE estimated from the Microwave Imagers for November–May between January 2006 and April 2007; **(B)** SWE from the DisUEB with TRMM precipitation, and **(C)** DisUEB with MPE for October 2006–April 2008. **(D)** Average SWE of the SNODAS and SNOTEL datasets for the period October 2006–April 2008.

HESSD
10, 3629–3664, 2013

Title Page
Abstract | Introduction
Conclusions | References
Tables | Figures
◄| |►
◄ ►
Back | Close
Full Screen / Esc
Printer-friendly Version
Interactive Discussion